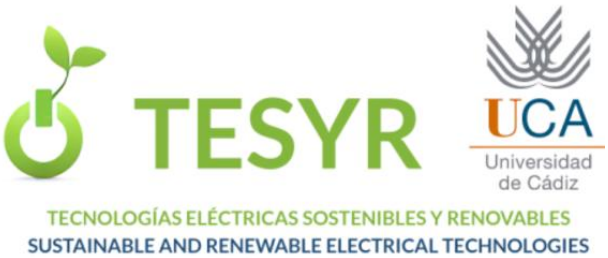

Universidad de Cádiz

Hierarchical Control for Isolated Microgrid Clusters Under Renewable Variability

Horrillo Quintero, Pablo; García Triviño, Pablo; Carrasco González, David; Sarrias Mena, Raúl; García Vázquez, Carlos Andrés; Fernández Ramírez, Luis Miguel

Published in:
Renewable Energy and Power Quality Journal: ICREPQ'25

ISBN (link to publication from Publisher):
https://www.icrepq.com/icrepq25/244-25%20horrillo.pdf

Publication date:
2025

Document Version:
Camera ready

Citation for published version:
P. Horrillo-Quintero, P. García-Triviño, D. Carrasco-González, R. Sarrias-Mena, C. A. García-Vázquez, and L. M. Fernández-Ramírez, “Hierarchical Control for Isolated Microgrid Clusters Under Renewable Variability,” Renewable Energy and Power Quality Journal: ICREPQ’25, pp. 1–6, Jul. 2025.

23rd International Conference on Renewable Energies and Power Quality (ICREPQ'25)
Tenerife (Spain), 25th to 27th June 2025
ISBN-13: 978-84-09-66511-2

Hierarchical Control for Isolated Microgrid Clusters Under Renewable Variability

P. Horrillo-Quintero[1], P. García-Triviño[1], D. Carrasco-González[1], R. Sarrias-Mena[2], C. A. García-Vázquez[1], L. M. Fernández-Ramírez[1]

[1] Department of Electrical Engineering
E.T.S.I.A University of Cadiz
Campus of Bahía de Algeciras – Algeciras, 11202 (Spain)

[2] Department of Engineering in Automation, Electronics, Computer Architecture & Networks
E.T.S.I.A University of Cadiz
Campus of Bahía de Algeciras – Algeciras, 11202 (Spain)

Abstract. This paper presents a novel hierarchical control for a microgrid cluster (MGC) operating in islanded mode, integrating renewable energy technologies (RETs), energy storage systems (ESSs), and variable demands. The control strategy dynamically manages power distribution by introducing the real-time available power concept, enabling proportional allocation of power among microgrids (MGs) based on their operational capacity. The proposed configuration includes MGs with grid-forming (GFM) inverters for voltage and frequency control and MGs with grid-following (GFL) inverter for power control. Unlike conventional methods that oversimplify the dynamics of RETs and ESSs, this approach ensures adaptive and reliable power sharing while addressing the challenges of intermittency and demand variability. Time-domain simulations across various operating scenarios validate the effectiveness of the proposed strategy, demonstrating its ability to maintain stable voltage and frequency in isolated MGCs. The results confirm the robustness and adaptability of the proposed hierarchical control framework, making it a viable solution for improving operational reliability and resilience in high-RETs penetration systems. This innovative approach advances the state of the art by providing a dynamic solution to manage the complexities of islanded MGC operations.

Key words. Isolated, microgrid-cluster, hierarchical, control, dynamic.

1. Introduction

Isolated microgrids (MGs) have long been considered viable alternatives in remote areas, capable of integrating a variety of distributed energy resources, including renewable energy technologies (RETs) and energy storage systems (ESSs) [1]. RETs, such as wind and solar photovoltaic (PV) technologies, contribute to low-inertia systems and are characterized by their intermittency due to weather conditions. This challenge is further amplified when multiple MGs are interconnected, forming a microgrid cluster (MGC), due to the varying operational states that may exist simultaneously across several MGs [2]. As a result, achieving coordinated control and ensuring frequency stability become essential for maintaining high-quality service in these systems.

In order to accomplish this objective, a hierarchical control architecture structured into three levels is commonly employed [3]. First, primary control provides a rapid response to fluctuations in demand, aiming to stabilize both the frequency and voltage of the system. However, operational disturbances such as variations in weather conditions, changes in the state of charge (SOC) of ESSs, or modifications in demand can lead to deviations in frequency and voltage, thereby compromising the stability of the MGC. To minimize these deviations, secondary control is implemented, with the responsibility of restoring the system's nominal values. Finally, at a higher level, tertiary control is responsible for establishing the operational references of each MG within the MGC, typically optimizing their operation according to a specific objective function [4].

Regarding current literature, several strategies have been explored for the control of MGs within this control framework. Reference [5] proposed a hierarchical cooperative control to address SOC equalization and precise current distribution among distributed ESSs and RETs in isolated direct current (DC) MGs. The primary control layer employed a logarithmic function to adaptively adjust the droop coefficient based on SOC, enabling fast equalization.

Reference [6] introduces a micro-market model for isolated MGs through optimization-based in a hierarchical approach. The model used a two-stage stochastic mixed-integer linear programming framework to schedule active and reactive power, as well as primary and secondary reserves, over a 24-hour horizon.

Regarding tertiary strategies, a non-linear model predictive control (MPC) strategy for tertiary control in DC MGs was proposed in [7]. However, variations in weather conditions during operation that could compromise the system's stability were not considered.

Reference [8] focused on optimizing tertiary-level control in MGC and introduced component life span as a new factor in energy management optimization. Case studies show that the proposed method can reduce operating costs by up to 62.91% compared to individual operation.
A novel fuzzy logic controller, with a focus on optimizing power exchange between isolated MGs was presented in [9]. The goal of the proposed supervisory control is to minimize fossil fuel consumption and reduce energy waste from power generation units.

One of the main challenges in the operation of MGCs is maintaining effective voltage and frequency control. With the increasing penetration of RETs and ESSs, this control is achieved through inverters operating as a grid-forming (GFM) converters, which are able to manage the variability of renewable generation, subject to the intermittency of weather conditions and fluctuations in demand. However, in several studies in the literature [5,10-12], it has been observed that the intermittency of generation in real-time control is often inadequately addressed, with RETs and ESSs modelled as ideal sources and the dynamic behavior of the systems being overlooked. This simplification can lead to suboptimal performance in frequency and voltage control when MGs operate in islanded mode.

To address these limitations, this paper introduces a hierarchical control strategy for a MGC operating in islanded mode in real-time. This approach is designed to adapt to the dynamic conditions of isolated power systems, ensuring effective voltage and frequency control. Unlike traditional models that oversimplify the dynamics of RETs and ESSs, the proposed strategy considers the variability of renewable generation, the SOC of ESSs, and fluctuating demand at both the MG and MGC levels. A key advancement is the introduction of the real-time available power concept within each MG, enabling a more accurate and flexible power allocation across the MGC. This allows the system to dynamically adjust to operational changes, maintaining stable frequency and voltage despite fluctuations in renewable generation and demand shifts.

The structure of this paper is organized as follows: Section 2 presents the isolated MGC under study, Section 3 introduces the proposed adaptive hierarchical control, Section 4 presents and discusses the simulation results, and Section 5 provides the conclusions.

2. Isolated Microgrid Cluster Under Study

A diagram illustrating the structure of the isolated MGC can be found in Fig. 1. The MGC is composed of three MGs, with two of them interlinked through GFM inverters.

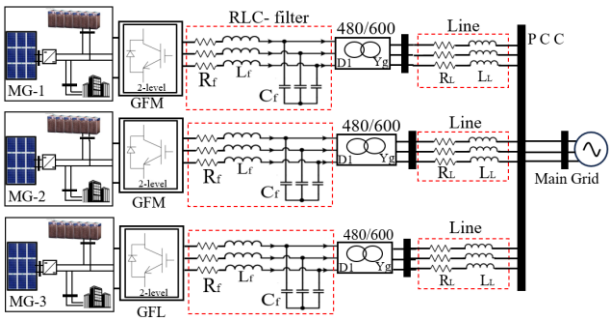

Fig. 1. MGC configuration.

A third one functions as a backup power source, linked via grid-forming inverter (GFL).
The PV model employed in this study follows the design detailed in [13]. The electrical characteristics of the PV model, specifically the current-voltage (I-V) curve, are calculated based on environmental factors such as irradiance and temperature. It comprises a diode, a current source regulated by a control unit, and two resistive elements. The PV system's operation is constrained by its maximum power point. The maximum power point tracking (MPPT) is achieved using the perturb and observe method, with a boost DC/DC converter integrated to optimize the energy extraction from the PV plant. The converter's duty cycle adapts dynamically in response to changes in irradiance, ensuring optimal power output from the PV generator. Additionally, a backup energy storage solution is provided by a lithium-ion battery energy storage system (BESS), which supports the PV plant. The BESS model used here is the one proposed in [14], which is incorporated into the SimPowerSystems toolbox in Simulink. To interconnect each MG with the point of common coupling (PCC), an RLC filter, an isolation transformer, and a transmission line, by incorporating an inductance and resistance into the system.

3. Hierarchical control

In this section, the hierarchical control designed for the MGC described in Section 2 is outlined. Fig. 2 presents a diagram of the hierarchical control levels. Initially, the primary control is based on droop control for MGs operating with GFM inverters and power control for MGs operating with GFD inverters. The frequency droop control is established according to:

$$f_i = f_{o,i} + n_{,i}(P_{o,i} - P_i) \quad (1)$$

in this case, f_i designates the MG frequency, $f_{o,i}$ specifies the reference frequency, n_i is the droop control factor, $P_{o,i}$ denotes the power corresponding to $f_{o,i}$, and P_i represents the active power supplied.

The voltage at the MG level can be determined as:

$$V_i = V_{o,i} - m_i Q_i \quad (2)$$

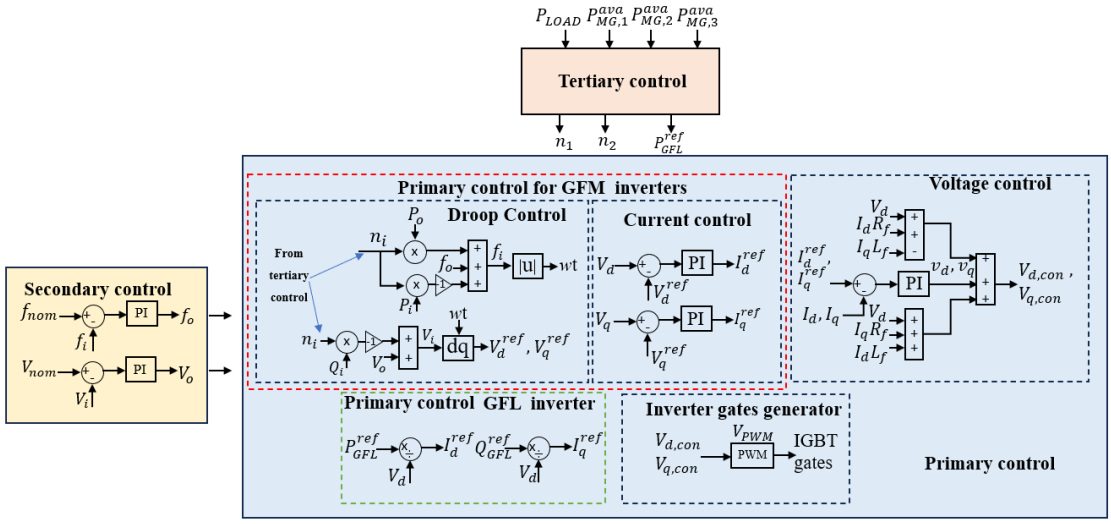

Fig. 2. Isolated MGC hierarchical control.

in Equation (2), V_i represents the terminal voltage, $V_{o,i}$ corresponds to the reference voltage value, m_i defines the droop coefficient for voltage, and Q_i indicates the reactive power delivered. It should be highlighted that for voltage droop regulation, $Q_{o,i}$ is assumed to be zero.

Subsequently, the primary control employs a cascaded architecture comprising a voltage regulation loop and a current regulation loop. The voltage regulation system ensures that the observed values of V_d and V_q align with their reference levels. A PI controller reduces the discrepancy between the actual voltages V_d, V_q and their respective reference values V_d^*, V_q^*. As a result, each PI controller produces the reference current, expressed as I_d^*, I_q^*.

The objective of the current regulation block is to ensure that the direct (I_d) and quadratic (I_q) currents align with their predefined setpoints, denoted as I_d^* and I_q^*. This is achieved through PI controllers, which generate the output signals $v_{d,i}$ and $v_{q,i}$, representing the voltage commands required for each inverter. Considering the inherent coupling between the 'd' and 'q' components, decoupling of these axes is essential. This is accomplished through feedforward compensation, which determines the direct and quadrature control voltages of the inverter ($V_{d,con}, V_{q,con}$) as follows:

$$V_{d,con} = V_d + I_d R_f - I_q L_f + v_{d,i} \quad (3)$$

$$V_{q,con} = V_d + I_d L_f + I_q R_f + v_{q,i} \quad (4)$$

in Equations (3) and (4), the resistance and inductance values associated with the filter are represented, respectively, as R_f and L_f. The pulse generation for each inverter is achieved using a conventional pulse width modulation (PWM) technique. To this end, the PWM module is responsible for generating the gate signals for the IGBTs, while concurrently regulating both the voltage and frequency in response to the active power output.

In the case of the MG employing a GFL inverter, the control strategy focuses on regulating a specific amount of power. Initially, a phase-locked loop (PLL) is utilized to capture the grid voltage (V_{abc}), allowing for the calculation of the angular frequency. Instead of relying on droop control, the system uses a power control strategy. The desired active power ($P_{GFI.}^*$) is normalized by the measured direct voltage V_d, generating the reference direct current I_d^*. Analogously, the reference for reactive power ($Q_{GFI.}^*$) is normalized by V_d to compute the reference quadrature current I_q^*. After calculating these parameters, the control operations are executed similarly to those for GFM inverters.

The role of the secondary control system is to correct the values of f_i and V_i, as the primary control does not ensure that these parameters are maintained in line with their desired reference points. This is accomplished by utilizing a PI controller to adjust the frequency f_o, which minimizes the difference between the actual measured frequency f_i and the nominal frequency f_{nom} of the MGC. Analogously, a PI controller is used to regulate V_o, which compensates for the discrepancy between the measured voltage V_i and the MGC's nominal voltage V_{nom}.

The tertiary control is developed to optimize the power allocation between MGs in real-time, ensuring that the operator's specifications are met. This approach is built upon the principle of power availability at any given moment. The available power for each MG ($P_{MG,n}^{ava}$) is determined by the following expression:

$$P_{MG,n}^{ava} = P_{PV,n} + P_{BESS,n} - P_{LOAD,n} \quad (5)$$

In this context, $P_{PV,n}$ represents the power output from the PV generator in every single MG, which is determined by the current solar radiation. The term $P_{BESS,n}$ corresponds to the available BESS power. Meanwhile, $P_{LOAD,n}$ indicates the local demand at the MG level.

In order to manage the charging and discharging cycles of the BESS, the following constrains are established:

$$P_{BESS,dis}^{max} = min\left(P_{BESS}^{rated}, \frac{E_{BESS}^{nom}}{\Delta t} \cdot \left(\frac{SOC - SOC_{min}}{100}\right)\right) \quad (6)$$

$$P_{BESS,ch}^{max} = min\left(P_{BESS}^{rated}, \frac{E_{BESS}^{nom}}{\Delta t} \cdot \left(\frac{SOC_{max} - SOC}{100}\right)\right) \quad (7)$$

The maximum discharge rate of the BESS is represented as $P_{BESS,dis}^{max}$ while the maximum charging rate is denoted by $P_{BESS,ch}^{max}$. The rated power of the BESS is indicated by P_{BESS}^{rated}. The expression $\frac{E_{BESS}^{nom}}{\Delta t}$ reflects the dynamic variation of the BESS energy over time. The minimum SOC allowed in the BESS is represented by SOC_{min}, and the maximum SOC permitted is represented by SOC_{min}.

The tertiary control is formulated as follows: initially, a minimum operational power, $P_{MG,3}^{res}$, is allocated to MG_3. Then, the total power to be distributed between MG_1 and MG_2, denoted as P_{SHARE}, is calculated as follows:

$$P_{SHARE} = P_{LOAD}^{MGC} - P_{MG,3}^{res} \quad (8)$$

in Equation (8), P_{LOAD}^{MGC} denotes the demand at the MGC level.

The allocation of power for MG_1 and MG_2 is carried out in proportion to the real-time available power of each MG. In the case that $P_{MG,1}^{ava} > P_{MG,2}^{ava}$, $MG_1$is required to manage a larger portion of power compared to MG_2. In order to accomplish this, the droop control coefficient of MG_1 (n_1) needs to be adjusted to a smaller value relative to that of MG_2 (n_2). On the other hand, if $P_{MG,1}^{ava}<P_{MG,2}^{ava}$ the power distribution is adjusted inversely.

After determining the droop control parameters, an initial power distribution among the MGs is obtained by calculating the power output for each one based on these parameters. The following step involves checking if the initial power distribution leads to any MG surpassing its available power capacity. In the event that the power of a particular MG, $P_{MG,n}$, exceeds its available capacity, $P_{MG,n}^{ava}$, the power output for that MG is constrained to the maximum available power, $P_{MG,n}^{ava}$, and any excess characterized as the imbalance between the initial distribution and $P_{MG,n}^{ava}$, is reassigned to MG_3. If there are no MGs that exceed their capacity, the initially calculated distribution is accepted as the final power allocation. In the final step, the power designated for MG_3 is determined by adding its required reserve power and any excess that MG_1 and MG_2 could not handle. If MG_3 lacks the capacity to absorb this additional power, the MGC will not be able to satisfy the load. As a result, the total manageable power is equivalent to the combined capacity of all the MGs.

4. Results and Discussion

This section presents a time-domain simulation to demonstrate the validity of the proposed hierarchical control for managing an islanded MGC, which accounts for the variability in renewable generation, as well as the load demand at both the MG and MGC levels. The MGC load is set as follows: 425 kW from 0 to 50 seconds, 255 kW from 50 to 100 seconds, 670 kW from 100 to 200 seconds, 560 kW from 200 to 230 seconds, 370 kW from 230 to 260 seconds, and finally 220 kW from 260 to 300 seconds. The initial SOC values are: SOC_1= 50%, SOC_2= 85%, and SOC_3= 40%.

For local loads at each MG, a load of 50 kW is considered for $MG_1$from 50 to 100 seconds, and a 50-kW load for MG_2 from 210 to 250 seconds. As a result of the local demand, the available capacity of the MGs to meet the MGC demand is reduced. Fig. 3 illustrates the irradiance profiles for the MGC. Specifically, Fig. 3a shows the irradiance for MG_1 (Irr_1), Fig. 3b shows the irradiance profile for MG_2 (Irr_2), and Fig. 3c shows the irradiance for MG_3 (Irr_3).

Fig. 4 illustrates the evolution of $P_{MG,n}^{ava}$ and $P_{MG,n}$. To demonstrate how the tertiary control allocates power between the MGs, two distinct scenarios are considered: one between 0 and 100 seconds, and the other between 100 and 250 seconds. In the initial 50 seconds, MG_1 provides an available power ($P_{MG,1}^{ava}$) of 350 kW, while MG_2 initially offers a value of $P_{MG,2}^{ava}$ = 309 kW, which increases to 341 kW at t=30 seconds. As the total available power from both MGs exceeds the MGC demand of 425 kW, MG_3 operates at its minimum power level. Consequently, $MG_1$and MG_2 assume the responsibility of meeting the demand. Specifically, MG_1contributes with 215 kW, and MG_2 provides 190 kW. The power balance is further adjusted with the contribution from MG_3, which delivers its minimum power of 20 kW.

When the local demand of $MG_1$is activated at t=50 seconds and variations in incident radiation occur, the value of $P_{MG,1}^{ava}$decreases to 270 kW, while $P_{MG,2}^{ava}$ remains at 341 kW. As a result, in this scenario where $P_{MG,2}^{ava}$> $P_{MG,1}^{ava}$, MG_2 assumes the responsibility of delivering a larger share of power to meet the demand. Specifically, MG_1delivers 104 kW, while MG_2 provides 131 kW.

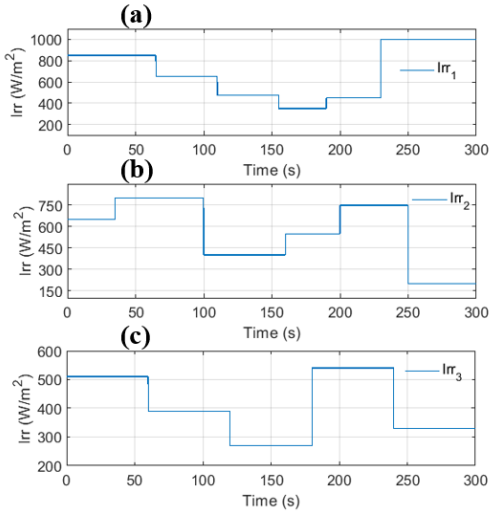

Fig. 3. Irradiation profile: (a) MG_1, (b) MG_2 and (a) MG_3.

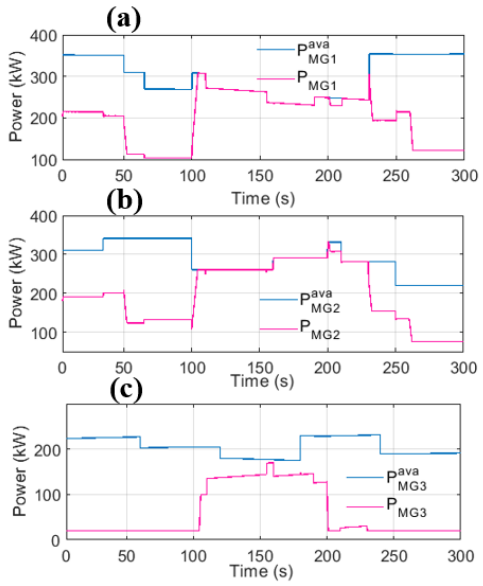

Fig. 4. MG capacity and delivered power: (a) MG1: $P^{ava}_{MG,1}$ and $P_{MG,1}$, (b) MG2: $P^{ava}_{MG,2}$ and $P_{MG,2}$ and (c) MG3: $P^{ava}_{MG,3}$ and $P_{MG,3}$.

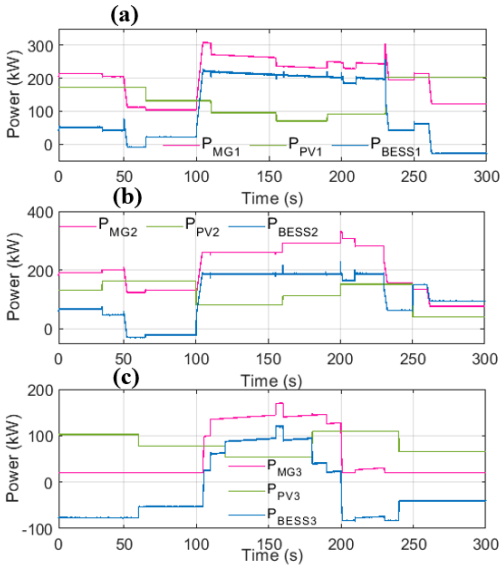

Fig. 5. MG powers: (a) MG1: $P_{MG,1}$, $P_{PV,1}$, $P_{BESS,1}$ (b) MG2: $P_{MG,2}$, $P_{PV,2}$, $P_{BESS,2}$ and (c) MG2: $P_{MG,3}$, $P_{PV,3}$, $P_{BESS,3}$.

Meanwhile, MG_3 continues to operate at its minimum power level, contributing 20 kW to complete the power balance. Together, they successfully meet the demand of 255 kW.

A particular scenario arises when the sum of the available capacities in MG_1 and MG_2 is insufficient to meet the demand, as occurs between 100 seconds and 200 seconds. During this interval, the demand of the MGC is 670 kW, decreasing to 560 kW from 200 seconds to 230 seconds. For instance, between 100s and 150s, the value of $P^{ava}_{MG,1}$is 268 kW, while $P^{ava}_{MG,2}$is 261 kW. Consequently, both MGs operate at their respective maximum available capacity, and MG_3 adjusts its operating mode, increasing its power output to 141 kW. When the available capacities of MG_1 and MG_2 exceed again the demand, as observed at 230 seconds, MG_3 returns to its minimum operating power, and the demand is distributed according to the previously outlined proportional allocation strategy. These results demonstrate that the tertiary control is able to effectively manage real-time power variations in each MG, which are directly influenced by the irradiance levels of each PV plant, and the activation of local loads.

Fig. 5 illustrates the power distribution at the MG level, comprising the values of $P_{MG,n}$, $P_{PV,n}$, and $P_{BESS,n}$. Particularly, Fig. 5a presents these power values for MG_1, Fig. 5b shows the power values for MG_2, and Fig. 5c displays the power values for MG_3.

In the first segment of the simulation, from 0 to 50 seconds, MG_1delivers 215 kW. The incident irradiance is 850 W/m², resulting in a $P_{PV,1}$ value of 172 kW, and the $P_{BESS,1}$ value is 43 kW. In the case of MG_2, it is required to provide 190 kW. With an irradiance value of 650 W/m², the $P_{PV,2}$ is 131 kW, and therefore, $P_{BESS,2}$ must contribute with 59 kW to meet the demand. Lastly, MG_3operates at its minimum operational level, delivering 20 kW. The incident irradiance for this PV generator is 510 W/m², which results in a $P_{PV,3}$value of 100 kW. Consequently, there is a surplus of power in this MG, which is managed through $BESS_3$, receiving 90 kW in charging mode. This operational mode persists over time, where it is observed that $BESS_1$ primarily operates in discharge mode between 0 and 100 seconds, due to the fact that $P_{PV,1}$ is lower than the power allocation that needs to be met. In contrast, for $BESS_2$, $P_{PV,2}$ exceeds the power delivered by this MG, causing $BESS_2$ to operate in charging mode.

Due to the increase in demand between 100 and 200 seconds, all BESSs operate in discharge mode to accommodate the demand and mitigate fluctuations in renewable generation. Subsequently, when the MGC demand decreases at 230 seconds to 370 kW, the operating conditions of each MG are adjusted accordingly. In this scenario, the renewable generation from MG_1amounts to 202 kW, while the allocated power for this MG is 122 kW. Therefore, the surplus of 80 kW is stored in $BESS_1$. In MG_2, a local load of 50 kW is connected, and the irradiance results in $P_{PV,2}$ being 152 kW. As a result, $BESS_2$ discharges 180 kW to meet both the local load and the power required by the tertiary control, which is 282 kW. In the final stage, MG_3 operates at its minimum power level, and the generated renewable power significantly exceeds this minimum, prompting $BESS_3$ to operate in charge mode once again.

Finally, Fig. 6 presents the frequency control (Fig. 6a) and voltage control (Fig. 6b) within the MGC. Due to the intermittency of renewable generation and the variability in both local MG demand and global demand, the MGC experiences disturbances that could potentially affect its stability. To mitigate this scenario, safety operational limits are defined, with a maximum frequency deviation of 0.5%, which corresponds to ± 0.3 Hz. For voltage, the

maximum allowed deviation is set to 4%, resulting in a maximum voltage of 624 V and a minimum voltage of 576 V. Fig. 6a shows that the maximum frequency deviation occurs at 100 seconds, when all MGs must discharge their BESS to meet the 670-kW load. The peak frequency reaches 60.19 Hz, while the minimum frequency reaches 59.82 Hz, thus remaining within the defined threshold of 59.7 Hz and 60.3 Hz. In Fig. 6b, the maximum voltage deviation is observed at 110 seconds, with a peak value of 609 V, while the minimum voltage is recorded at 590 V at 200 seconds. In both cases, the values remain within the established operating thresholds.

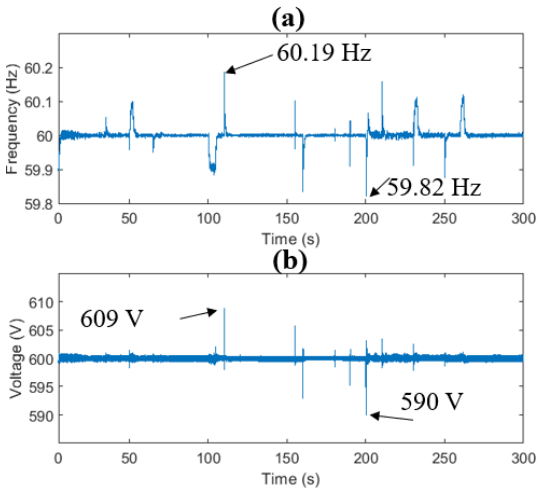

Fig. 6. (a) MGC frequency and (b) MGC voltage at PCC.

5. Conclusion

This article introduced a hierarchical control framework for a MGC operating in islanded mode, addressing the challenges posed by the variability of renewable energy generation, fluctuating demand, and the dynamic constraints of ESSs. Unlike conventional approaches that often simplify the dynamic behavior of RETs and ESSs, this strategy accounted for weather conditions and variability both MG and MGC levels. A significant contribution was the incorporation of the real-time available power concept, enabling proportional power allocation among MGs based on their operational capacity. This innovative ensured a stable voltage and frequency control despite the inherent uncertainties of islanded systems. The proposed MGC is built upon RETs, such as PV power plants and BESS, which are inherently modular and easily scalable. This modular nature allows for seamless expansion by integrating additional generation and storage units without requiring extensive reconfiguration of the existing infrastructure. Furthermore, the proposed control approach employs generic measures, such as available power, to effectively manage the system, enabling it to accommodate an increasing number of interconnected microgrids while maintaining operational stability and efficiency. As a result, the approach can be effectively scaled to larger microgrid networks, ensuring adaptability to varying energy demands and system configurations.

Acknowledgement

This work was partially supported by Ministerio de Ciencia e Innovación, Agencia Estatal de Investigación, FEDER, UE (Grant PID2021-123633OB-C32 supported by MCIN/AEI/10.13039/501100011033/FEDER, UE).

References

[1] Machele IL, Onumanyi AJ, Abu-Mahfouz AM, Kurien AM. Interconnected Smart Transactive Microgrids—A Survey on Trading, Energy Management Systems, and Optimisation Approaches. Journal of Sensor and Actuator Networks 2024;13. https://doi.org/10.3390/jsan13020020.
[2] Suryani A, Sulaeman I, Rosyid OA, Moonen N, Popovic J. Interoperability in Microgrids to Improve Energy Access: A Systematic Review. IEEE Access 2024;12:64267–84. https://doi.org/10.1109/ACCESS.2024.3396275.
[3] Li S, Oshnoei A, Blaabjerg F, Anvari-Moghaddam A. Hierarchical Control for Microgrids: A Survey on Classical and Machine Learning-Based Methods. Sustainability (Switzerland) 2023;15. https://doi.org/10.3390/su15118952.
[4] Al-Ismail FS. A Critical Review on DC Microgrids Voltage Control and Power Management. IEEE Access 2024;12:30345–61. https://doi.org/10.1109/ACCESS.2024.3369609.
[5] Xie C, Wei M, Luo D, Yang L. Energy balancing strategy for the multi-storage islanded DC microgrid based on hierarchical cooperative control. Front Energy Res 2024;12. https://doi.org/10.3389/fenrg.2024.1390621.
[6] Abedi T, Yousefi G, Shafie-Khah M. Hierarchical Stochastic Frequency Constrained Micro-Market Model for Isolated Microgrids. IEEE Trans Smart Grid 2024;15:5–18. https://doi.org/10.1109/TSG.2023.3266761.
[7] Ramirez-Marin SA, Garcés-Ruiz A, Cortés-Borray AF, Perez-Basante A, Rodríguez-Seco JE. Model-predictive control with admittance matrix estimation for the optimal power sharing in isolated DC microgrids. Electric Power Systems Research 2025;241. https://doi.org/10.1016/j.epsr.2024.111380.
[8] Rashidi R, Hatami A, Abedini M. Multi-microgrid energy management through tertiary-level control: Structure and case study. Sustainable Energy Technologies and Assessments 2021;47. https://doi.org/10.1016/j.seta.2021.101395.
[9] Rodriguez M, Arcos-Aviles D, Guinjoan F. Simple fuzzy logic-based energy management for power exchange in isolated multi-microgrid systems: A case study in a remote community in the Amazon region of Ecuador. Appl Energy 2024;357. https://doi.org/10.1016/j.apenergy.2023.122522.
[10] Soofi M, Jalilvand A, Delavari H, Mobayen S, Su C-L. Prescribed Performance Control Strategy for an Isolated Multi-Agent DC Microgrid. IEEE Trans Smart Grid 2024:1–1. https://doi.org/10.1109/tsg.2024.3456234.
[11] Liu Y, Yang L, Wei M. A novel droop coefficient to realize rapid SOC balance for distributed energy storage systems. International Journal of Electrical Power and Energy Systems 2025;164. https://doi.org/10.1016/j.ijepes.2024.110398.
[12] Sadeque F, Gursoy M, Mirafzal B. Grid-Forming Inverters in a Microgrid: Maintaining Power During an Outage and Restoring Connection to the Utility Grid Without Communication. IEEE Transactions on Industrial Electronics 2024;71:11796–805. https://doi.org/10.1109/TIE.2024.3349574.
[13] Mathworks. PV array. Online. Available: https://es.mathworks.com/help/sps/powersys/ref/pvarray.html
[14] Mathworks. Battery. Online. Available: https://es.mathworks.com/help/sps/powersys/ref/battery.html